metals

MDPI

Article

MgAl Oxide Coatings Modified with CeO_2 Particles Formed by Plasma Electrolytic Oxidation of AZ31 Magnesium Alloy: Photoluminescent and Photocatalytic Properties

Stevan Stojadinović [1,2,*] and Nenad Radić [3]

[1] Faculty of Physics, University of Belgrade, Studentski trg 12-16, 11000 Belgrade, Serbia
[2] Faculty of Forestry, University of Belgrade, Kneza Višeslava 1, 11000 Belgrade, Serbia
[3] IChTM-Department of Catalysis and Chemical Engineering, University of Belgrade, Njegoševa 12, 11000 Belgrade, Serbia; nradic@nanosys.ihtm.bg.ac.rs
* Correspondence: sstevan@ff.bg.ac.rs; Tel.: +381-11-7158161

Abstract: MgAl oxide coatings composed of MgO and $MgAl_2O_4$ phases were doped with CeO_2 particles via plasma electrolytic oxidation (PEO) of AZ31 magnesium alloy in a 5 g/L $NaAlO_2$ water solution. Subsequently, particles of CeO_2 up to 8 g/L were added. Extensive investigations were conducted to examine the morphology, the chemical and phase compositions, and, most importantly, the photoluminescent (PL) properties and photocatalytic activity (PA) during the photodegradation of methyl orange. The number of CeO_2 particles incorporated into MgAl oxide coatings depends on the concentration of CeO_2 particles in the aluminate electrolyte. However, the CeO_2 particles do not significantly affect the thickness, phase structure, or surface morphology of the coatings. The PL emission spectrum of MgAl oxide coatings is divided into two bands: one in the 350–600 nm range related to structural defects in MgO, and another much more intense band in the 600–775 nm range attributed to the F^+ centres in $MgAl_2O_4$. The incorporated CeO_2 particles do not have a significant effect on the PL intensity of the band in the red spectral region, but the PL intensity of the first band increases with the concentration of CeO_2 particles. The PA of MgAl/CeO_2 oxide coatings is higher than that of pure MgAl oxide coatings. The MgAl/CeO_2 oxide coating developed in aluminate electrolyte with a concentration of 2 g/L CeO_2 particles exhibited the highest PA. The MgAl/CeO_2 oxide coatings remained chemically and physically stable across multiple cycles, indicating their potential for applications.

Keywords: plasma electrolytic oxidation; photocatalysis; photoluminescence; MgO; $MgAl_2O_4$; CeO_2; methyl orange

Citation: Stojadinović, S.; Radić, N. MgAl Oxide Coatings Modified with CeO_2 Particles Formed by Plasma Electrolytic Oxidation of AZ31 Magnesium Alloy: Photoluminescent and Photocatalytic Properties. *Metals* **2024**, *14*, 366. https://doi.org/10.3390/met14030366

Academic Editors: Claudia Barile and Gilda Renna

Received: 27 February 2024
Revised: 18 March 2024
Accepted: 19 March 2024
Published: 21 March 2024

1. Introduction

Plasma electrolytic oxidation (PEO) is an eco-friendly electrochemical surface treatment that produces highly stable oxide coatings on a variety of metals (Mg, Al, Ti, Ta, Nb, Zr) and their alloys with a high crystallinity, substrate adhesion, and physical, chemical, and thermal stability [1–4]. PEO necessitates a high anodic voltage (several hundred volts) to promote the local dielectric breakdown of the growing oxide film, resulting in numerous short-lived micro-discharges formed continuously over the metal electrode surface [5]. The breakdown process entails intricate electrochemical, thermal, and plasma processes that incorporate both metal and electrolyte components into coatings.

Magnesium and magnesium alloys are desirable materials for practical applications due to their low density; high strength-to-weight ratio; excellent dimensional stability, biodegradability, and biocompatibility; large hydrogen storage capacity; high specific capacity for batteries; good electromagnetic shielding; high machinability; and so on [6,7]. The foremost drawback of magnesium-based materials is their poor resistance to corrosion, which limits their application [8]. Magnesium and its alloys' surfaces are commonly

modified to improve their corrosion resistance and to create functional coatings suitable for various applications [9].

Lately, PEO has become increasingly popular as a method for producing multifunctional coatings and improving the surface characteristics of magnesium and its alloys [10–18]. Some studies have shown that oxide coatings formed on magnesium alloys can be used in photocatalytic applications [19–23]. The present study focuses on the investigation of the photoluminescent (PL) and photocatalytic properties of coatings formed via PEO of AZ31 magnesium alloy in aluminate electrolyte with the addition of CeO_2 particles at different concentrations. PEO formed coatings on AZ31 magnesium alloys in aluminate electrolytes containing MgO and $MgAl_2O_4$ phases [22]. Both of these phases have found application in photocatalysis [24,25] and as hosts for photoluminescence materials [26,27] due to the presence of different types of oxygen vacancies and other defects.

Adding CeO_2 particles to the electrolyte causes their incorporation into the coatings during PEO in magnesium alloys, which improves their corrosive properties and resistance to wear [28,29]. This is critical in engineering applications involving oxide coatings on magnesium alloys. The main idea behind this work was to create $MgO/MgAl_2O_4/CeO_2$ coatings in order to improve the photocatalytic and PL properties of a single $MgO/MgAl_2O_4$ coating and optimize the amount of CeO_2 particles in the electrolyte. The properties of CeO_2, such as its low toxicity, strong oxygen storage capacity, high chemical stability, and ability to display dual oxidation states of cerium, Ce^{3+}/Ce^{4+}, have drawn a lot of attention in the field of photocatalysis due to the formation of abundant oxygen vacancies in CeO_2, which serve as active electron trap centres, inhibiting recombination of photogenerated electron/hole pairs [30–34].

The photocatalytic and PL properties of the MgO/CeO_2 and $MgAl_2O_4/CeO_2$ systems have received little attention in the literature [35–37], with no data available for the $MgO/MgAl_2O_4/CeO_2$ system. Our study has, for the first time, shown that PEO applied to magnesium alloys can generate $MgO/MgAl_2O_4/CeO_2$ coatings suitable for photocatalytic and PL applications. Consequently, the $MgO/MgAl_2O_4/CeO_2$ coatings formed by PEO were examined using SEM/EDS, XRD, Raman spectroscopy, and DRS to investigate the effect of CeO_2 on the morphology, chemical composition, crystal structure, and absorption properties of $MgO/MgAl_2O_4/CeO_2$. The PL of the $MgO/MgAl_2O_4/CeO_2$ coatings was thoroughly investigated, as the incorporation of CeO_2 into $MgO/MgAl_2O_4$ coatings increases the PL intensity by more than an order of magnitude. The photocatalytic efficiency of the coatings was evaluated through the degradation of methyl orange (MO) dye. MO is an example of a typical azo-anionic dye, which is hard to degrade, hazardous to the environment, and potentially dangerous to human health if it finds its way into soil and water resources.

2. Materials and Methods

The starting material for the preparation of PEO coatings was a rectangular sample (25 mm × 10 mm × 0.81 mm) of AZ31 magnesium alloy (96% Mg, 3% Al, 1% Zn, Alfa Aesar, Ward Hill, MA, USA). Ultrasonic cleaning using acetone and subsequent drying with a warm air stream were included in the sample preparation process for PEO. After this, the samples were coated with an insulating resin, ensuring that the electrolyte only made contact with the 15 mm × 10 mm active surface.

The electrolytic cell was made of double-walled glass and cooled with water (refer to Figure 10 in ref. [22]). A magnetic stirrer was employed to mix the electrolyte in the electrolytic cell, ensuring the even distribution of CeO_2 particles. A tubular stainless-steel cathode was positioned around the anode samples of AZ31 magnesium alloy, which were used and positioned in the centre of the electrolytic cell. The electrolyte solution was prepared by adding CeO_2 particles at concentrations of 1 g/L, 2 g/L, 4 g/L, and 8 g/L into a water solution containing 5 g/L of $NaAlO_2$. The PEO processes were conducted using a DC power source (Consort EV261) at a constant current density of 150 mA/cm^2 for 10 min. The electrolyte temperature was maintained at (20 ± 1) °C. Following the PEO

process, samples were rinsed with distilled water to prevent the accumulation of electrolyte components during the drying process.

The morphology, thickness, elemental, and phase analyses of the PEO coatings were performed using a scanning electron microscope (SEM, JEOL 840A, Tokyo, Japan) with energy-dispersive X-ray spectroscopy (EDS, Oxford INCA, Abingdon, UK), X-ray diffraction (XRD, Rigaku Ultima IV, Tokyo, Japan), and Raman spectroscopy (TriVista 557 Raman system, S&I GmbH, Germany). UV-Vis diffuse reflectance spectra (DRS) were employed, utilizing a Shimadzu UV-3600, Tokyo, Japan, to analyse the optical properties of the PEO coatings. To acquire room temperature PL excitation and emission spectra, a spectrofluorometer (Horiba Jobin Yvon, Fluorolog FL3-22, Edison, NJ, USA) was utilized with a 450 W xenon lamp as the excitation source.

To assess the photocatalytic activity (PA) of the coatings, the photodegradation of MO, serving as a model compound for organic pollution, was carried out at 20 °C under simulated artificial solar radiation. A photocatalytic reactor featuring double-walled glass with water cooling was utilized (see Figure 1 in ref. [38]). The samples were positioned on the stainless-steel holder, 5 mm above the bottom of the photocatalytic reactor. A magnetic stirrer that was positioned underneath the holder was used to mix the 10 cm^3 solution of MO. The MO concentration was 8 mg/L at first. The samples were exposed to illumination from a 300 W light source (OSRAM ULTRA-VITALUX UV-A, Munich, Germany) positioned 25 cm above the solution's upper surface. To achieve an adsorption–desorption equilibrium, the initial MO solution and samples were left in the dark for an hour prior to illumination. PA was assessed by monitoring the decomposition of MO following an appropriate duration of light exposure. The maximum absorption peak of MO at 464 nm was measured utilizing a UV-Vis spectrometer (Thermo Electron Nicolet, Evolution 500, Cambridge, UK). The absorbance was transformed into MO concentration utilizing a standard curve that exhibited a linear correlation between concentration and absorbance at this wavelength.

3. Results and Discussion

Figure 1 illustrates the voltage–time characteristics observed during the anodization process of AZ31 magnesium alloy in a solution containing 5 g/L $NaAlO_2$, both with and without the addition of 8 g/L CeO_2 particles. As shown, the inclusion of CeO_2 particles did not produce any noticeable impact on the voltage–time curves, with two distinct regions being identifiable. The first region is linked to classical anodization and the formation of a thin dense oxide layer, characterized by an almost linear rise in voltage. The second region is correlated with dielectric breakdown of the formed compact oxide layer, indicated by a noticeable deviation from the linearity of the voltage–time curve and the occurrence of numerous micro-discharges.

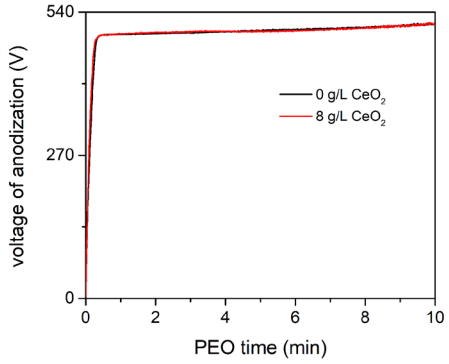

Figure 1. Voltage–time curves during anodization in 5 g/L $NaAlO_2$ without and with 8 g/L of CeO_2 particles.

Figure 2 displays the top view and cross-section SEM micrographs of the coating created in 5 g/L $NaAlO_2$ with different concentrations of added CeO_2 particles. Changing

the concentration of CeO_2 particles had no discernible effect on the surface morphology or coating thickness. All coatings share a common morphology, defined by the presence of molten regions dispersed throughout the surface created when the molten oxide heats up, melts, and then cools down in contact with the surrounding electrolyte and pores originating from gas bubbles released during the PEO [39]. The coatings formed after 10 min of PEO are about (22 ± 1) μm thick.

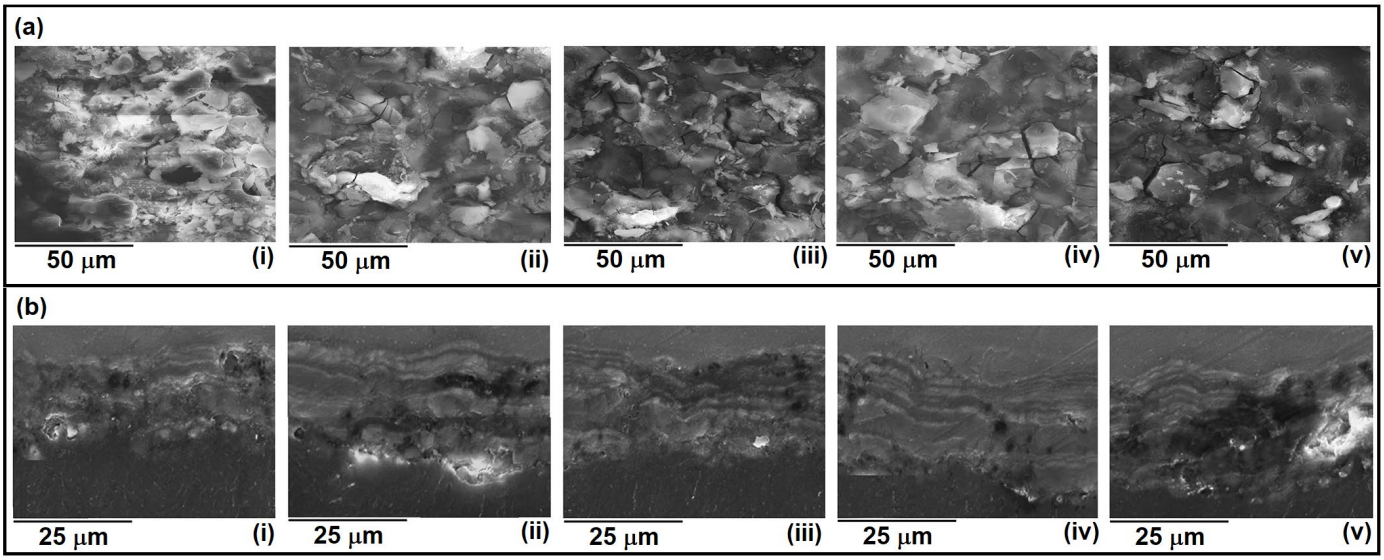

Figure 2. (**a**) Top view and (**b**) cross-section micrographs of coatings formed in 5 g/L $NaAlO_2$ by adding CeO_2 particles in concentrations of (**i**) 0 g/L; (**ii**) 1 g/L; (**iii**) 2 g/L; (**iv**) 4 g/L; (**v**) 8 g/L.

The results of the integrated EDS analysis of the coatings are given in Table 1 (the relative errors are less than 5%). The coatings' chemical constituents are Mg, Al, O, and Ce. The electrolyte is the main source of Al. Small amounts of Ce are present in the coatings, which increases with the concentration of CeO_2 particles in the electrolyte.

Table 1. Integrated EDS analysis of coatings in Figure 2a formed in 5 g/L $NaAlO_2$ with varying concentrations of CeO_2 particles added.

CeO_2 (g/L)	Atomic (%)			
	O	Mg	Al	Ce
0	65.44	14.02	20.54	/
1	65.53	14.79	19.63	0.05
2	64.52	15.76	19.61	0.11
4	64.84	15.91	19.02	0.23
8	64.43	15.85	19.32	0.40

The XRD patterns of PEO coatings formed in 5 g/L $NaAlO_2$ with different concentrations of CeO_2 particles, along with the XRD patterns of pure CeO_2 particles and the AZ31 magnesium alloy substrate, are displayed in Figure 3a. The XRD pattern of CeO_2 particles reveals peaks at 2θ values of 28.7, 33.2, 47.6, 56.4, 59.2, 69.5, 76.8, and 79.2 degrees, corresponding to the (111), (200), (220), (311), (222), (400), (331), and (420) crystalline planes of the cubic fluorite structure of CeO_2 (JCPDS Card No. 75-0162). The formation of MgO (JCPDS card No. 79-0612) and $MgAl_2O_4$ (JCPDS card No. 77-0435) phases, as a result of an interaction between the AZ31 substrate and the electrolyte components, is confirmed by the XRD pattern of the PEO coating formed in 5 g/L $NaAlO_2$ [22]. The significant diffraction peaks observed from the substrate are a result of X-ray penetration through the porous oxide layer and subsequent reflection from the substrate. The diffraction peaks of CeO_2 can be clearly seen together with the diffraction peaks arising from MgO and $MgAl_2O_4$

in the XRD patterns of the PEO coatings formed in 5 g/L $NaAlO_2$ with the addition of a high concentration of CeO_2 particles (4 g/L and 8 g/L). This is primarily due to the low concentration of evenly distributed CeO_2 particles throughout the surface coatings [22,23].

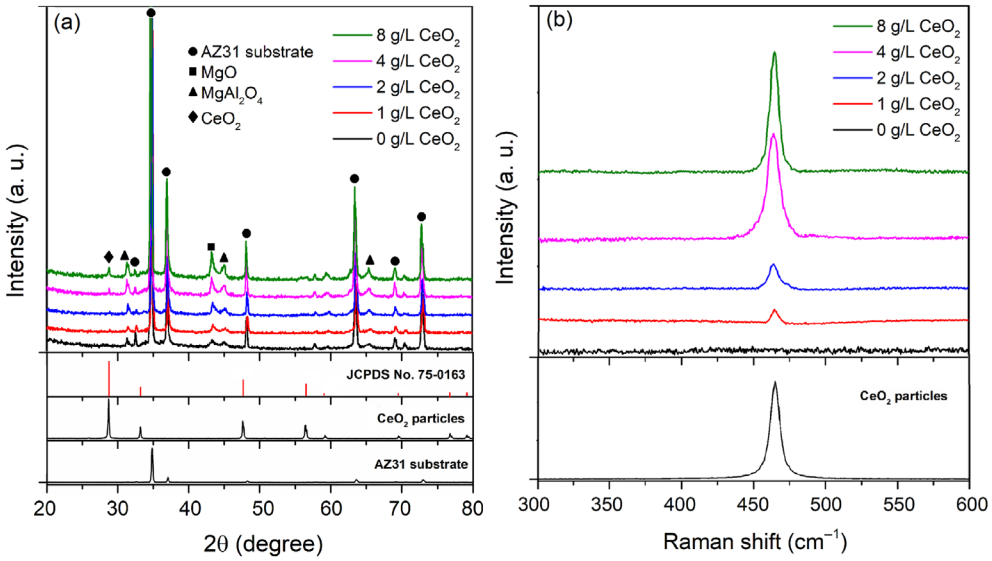

Figure 3. (**a**) XRD patterns and (**b**) Raman spectra of coatings formed in 5 g/L $NaAlO_2$ with varying concentrations of CeO_2 particles.

Raman measurements were conducted (Figure 3b) to verify the presence of CeO_2 particles in the PEO coatings formed in a solution containing 5 g/L $NaAlO_2$ with the addition of lower concentrations of CeO_2 particles (1 g/L and 2 g/L). The F_{2g} mode of the cubic fluorite structure of CeO_2, identified as the prominent band in the Raman spectrum of CeO_2 particles around 465 cm^{-1}, is attributed to the symmetrical vibration of oxygen atoms surrounding Ce^{4+} [40]. All coatings formed in a solution containing 5 g/L $NaAlO_2$ with the inclusion of CeO_2 particles exhibit this mode in their Raman spectra, suggesting the integration of CeO_2 particles into the coatings.

PEO facilitates the inclusion of electrolyte particles into coatings in three distinct forms: partially reactive, reactive, and inert forms [41]. The two main factors that determine the mode of incorporation are the melting point and the particle size. An inert mode of incorporation typically applies to particles with high melting points, such as CeO_2 (approximately 2400 °C) [42], which is also applicable in our case.

PL excitation and emission spectra of the MgO/$MgAl_2O_4$ coatings are shown in Figure 4. The PL emission spectrum excited at 265 nm (Figure 4a) is characterized by a strong emission band in the red region with a maximum of about 720 nm, related to F^+ centres in $MgAl_2O_4$ [43], and a broad band in the range of 350 nm to 600 nm, which is associated with oxygen vacancies (e.g., F, F^+, F_2, and F_2^{2+} centres) mostly in MgO [44,45]. Upon excitation at 340 nm (Figure 4b), two PL bands with peak positions at about 410 nm and 660 nm can be observed in the PL emission spectrum, which are related to oxygen vacancies in MgO [21].

The incorporation of CeO_2 particles into MgO/$MgAl_2O_4$ coatings does not notably impact the photoluminescence (PL) intensity of the band peaking around 720 nm under 265 nm excitation. However, it does lead to a significant increase in the PL intensity of the broad band, with a maximum of around 410 nm (Figure 5a). The PL emission spectra, excited at 340 nm, further reveal that the PL intensity of the band peaking around 410 nm increases with the concentration of CeO_2 particles incorporated into the MgO/$MgAl_2O_4$ coatings (Figure 5b). The ratio of PL intensity of coatings formed in a solution containing 5 g/L $NaAlO_2$ with and without 8 g/L CeO_2 particles is approximately 20. In addition to this PL band, a PL band with a maximum at around 520 nm, as well as PL bands in the red region with a weak intensity, can be observed in the PL emission spectra (Figure 5a,b).

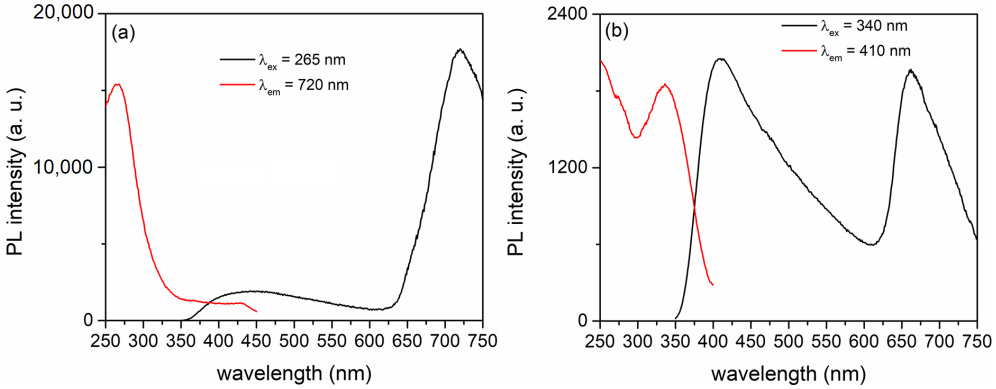

Figure 4. PL excitation and emission spectra of $MgO/MgAl_2O_4$ coatings: (**a**) λ_{ex} = 265 nm, λ_{em} = 720 nm; (**b**) λ_{ex} = 340 nm, λ_{em} = 410 nm.

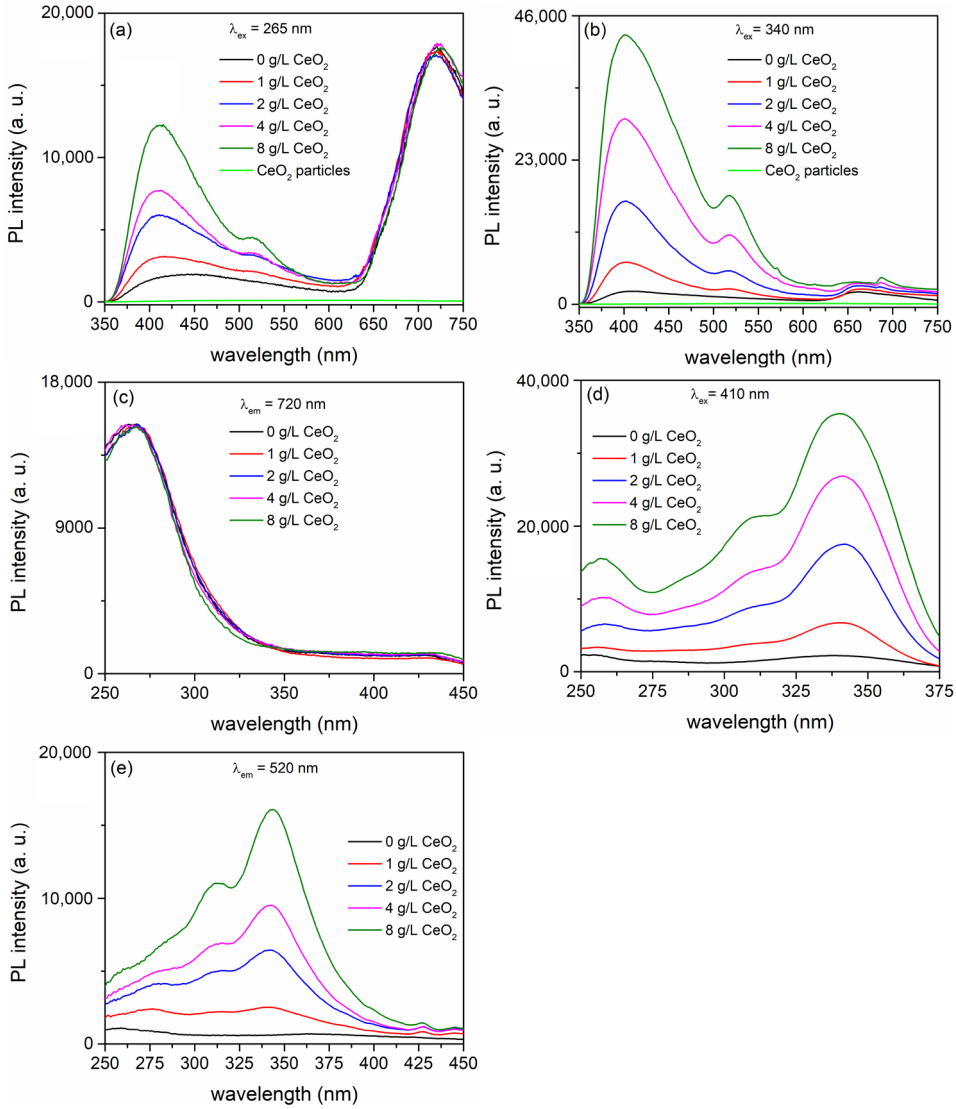

Figure 5. PL spectra of $MgO/MgAl_2O_4/CeO_2$ coatings formed in 5 g/L $NaAlO_2$ with varying concentrations of CeO_2 particles: (**a**) emission spectra excited at 265 nm; (**b**) emission spectra excited at 340 nm; (**c**) excitation spectra monitored at 720 nm; (**d**) excitation spectra monitored at 410 nm; (**e**) excitation spectra monitored at 520 nm.

The PL excitation spectra of $MgO/MgAl_2O_4/CeO_2$ coatings monitored at 720 nm consist of one intense band with a maximum of around 265 nm (Figure 5c). The content

of CeO_2 in the $MgO/MgAl_2O_4/CeO_2$ coatings does not affect the PL intensity of this band, which is in agreement with the corresponding PL emission spectra in Figure 4a. PL excitation spectra of $MgO/MgAl_2O_4/CeO_2$ coatings monitored at 410 nm and 520 nm consist of at least three bands at about 265 nm, 315 nm, and 340 nm (Figure 5c,d). Among these excitation transitions, the one at 340 nm is the most intense.

The increase in the PL intensity of $MgO/MgAl_2O_4/CeO_2$ coatings compared to pure $MgO/MgAl_2O_4$ is due to the creation of oxygen vacancies as a result of the incorporation of CeO_2, because the PL originating from CeO_2 particles is negligible. Bands with maxima at around 410 nm and 520 nm are attributed to F^+ and F centres, respectively [46–48].

Figure 6a illustrates how the concentration of CeO_2 particles in the electrolyte affects the MO photodegradation efficiency using the formed coatings. C_0 is the initial concentration of MO, and its concentration at time t is C. For every CeO_2 concentration, three samples were examined, and the mean values are displayed in Figure 6a. Samples collected under identical conditions have a very high reproducibility (within 3%) for the PA. The concentration of CeO_2 particles added to the electrolyte affects the PA of the $MgO/MgAl_2O_4/CeO_2$ coatings, which is significantly higher than that of $MgO/MgAl_2O_4$ coatings. The highest PA of $MgO/MgAl_2O_4/CeO_2$ coatings was achieved with the addition of 2 g/L of CeO_2 particles.

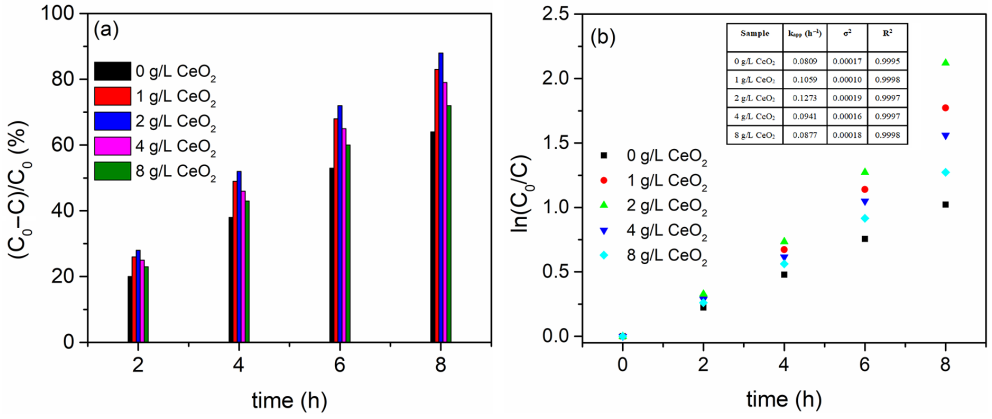

Figure 6. (**a**) PA and (**b**) first-order kinetic plots of coatings formed in 5 g/L $NaAlO_2$ with varying concentrations of CeO_2 particles.

The first-order kinetic Langmuir Hinshelwood model (Figure 6b) provides a good description of the photocatalytic degradation of MO:

$$ln\left(\frac{C_o}{C}\right) = k_{app}t \quad (1)$$

The table in Figure 6b presents the first-order kinetic constant k_{app}, along with the corresponding standard squared deviation (σ) and linear correlation coefficient (R^2). The value of k_{app} was determined through non-linear least squares fitting conducted across the entire experimental time range [49]. As the concentration of CeO_2 particles in the aluminate electrolyte increased up to 2 g/L, the degradation rate constant k_{app} increased from 0.0809 h^{-1} to 0.1273 h^{-1}. The sensitivity of MO degradation to the content of CeO_2 in $MgO/MgAl_2O_4/CeO_2$ coatings was confirmed by a decrease in the degradation rate constant with the increase in the concentration of CeO_2 in the aluminate electrolyte up to 8 g/L.

CeO_2 particles have a very low PA in organic dye degradation due to the rapid recombination of photogenerated electron/hole pairs [50]. Because the concentration of CeO_2 particles in the formed $MgO/MgAl_2O_4/CeO_2$ coatings is so low, the contribution of CeO_2 particles to the total PA of these coatings is negligible. Since the morphology, thickness, and phase structure of all the $MgO/MgAl_2O_4/CeO_2$ coatings are essentially the same (Figures 2 and 3), CeO_2 particles contribute to the increasing PA of $MgO/MgAl_2O_4$

coatings primarily by extending their optical absorption range or by decreasing the prompt recombination of photogenerated electron/hole pairs.

The UV–Vis DRS spectra of CeO_2 particles and the formed coatings are shown in Figure 7. A broad absorption band in the mid-UV region is typical for $MgO/MgAl_2O_4$ formed in an aluminate electrolyte [22]. The used CeO_2 particles have an absorption band edge at approximately 440 nm. Due to the low concentration of CeO_2 in the formed coatings, the shift in the absorption curves towards the visible region is insignificant, especially for low concentrations of CeO_2 particles in the electrolyte (1, 2, and 4 g/L). This indicates that the increased PA of $MgO/MgAl_2O_4/CeO_2$ coatings compared to $MgO/MgAl_2O_4$ coatings is due to a decrease in photogenerated electron/hole recombination rate as a result of $MgO/MgAl_2O_4$ and CeO_2 coupling.

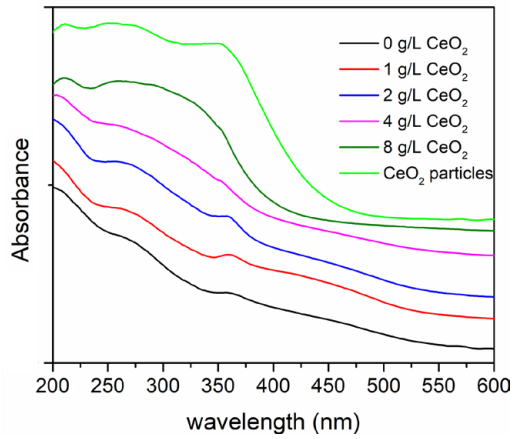

Figure 7. DRS spectra of CeO_2 particles and coatings formed in 5 g/L $NaAlO_2$ with varying concentrations of CeO_2 particles added.

PL and PA measurements indicate that the high concentration of various types of oxygen vacancies and other defects is related to the significant PA of $MgO/MgAl_2O_4/CeO_2$ coatings. The formation of oxygen vacancies during PEO introduces defect states within the material's bandgap, facilitating photogenerated charge carrier separation and causing an increase in the PA of $MgO/MgAl_2O_4/CeO_2$ coatings formed in aluminate electrolyte with the addition of CeO_2 particles in relation to $MgO/MgAl_2O_4$ coatings formed in a pure aluminate electrolyte. The PA of $MgO/MgAl_2O_4/CeO_2$ coatings varies with the concentration of CeO_2 particles in the aluminate electrolyte. The $MgO/MgAl_2O_4/CeO_2$ coating which was formed in the aluminate electrolyte with 2 g/L CeO_2 particles had the highest PA. As the concentration of CeO_2 in the aluminate electrolyte continues to increase, the PA decreases because CeO_2 particles serve as photoinduced electron capture centres [51].

Ten consecutive photocatalytic tests were conducted on the most active photocatalyst in order to investigate the potential application of $MgO/MgAl_2O_4/CeO_2$ coatings in photocatalysis. Figure 8 shows the recycling test of MO photodegradation along with the morphology and composition before and after 10 runs. The morphology, composition, and PA did not change, indicating that the produced photocatalyst exhibited a high degree of chemical and physical stability.

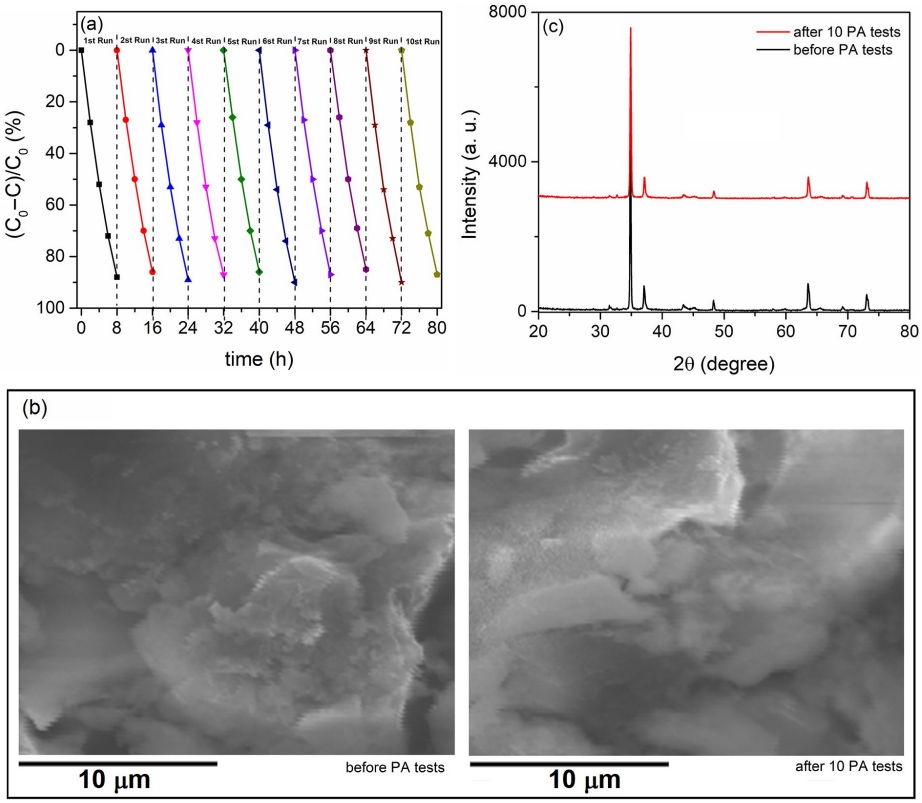

Figure 8. (**a**) MO photodegradation recycling experiment; (**b**) SEM micrographs before and after 10 cycles; and (**c**) XRD patterns before and after 10 cycles of a coating formed in 5 g/L $NaAlO_2$ + 2 g/L CeO_2.

4. Conclusions

PEO of AZ31 magnesium alloy in an aluminate electrolyte with the addition of CeO_2 particles at different concentrations was utilized to create $MgO/MgAl_2O_4/CeO_2$ coatings. To examine the morphology, crystal structure, chemical composition, and optical and PL properties of the formed coatings, various techniques, including SEM/EDS, XRD, Raman spectroscopy, XPS, DRS, and PL, were employed. The photodegradation of MO under simulated sunlight was employed to evaluate the photocatalytic potential of $MgO/MgAl_2O_4/CeO_2$ coatings.

The results can be summarized as follows:

- The surface morphology, thickness, phase structure, and light-harvesting characteristics of $MgO/MgAl_2O_4/CeO_2$ coatings are not significantly affected by the addition of CeO_2 particles to the aluminate electrolyte.
- As a result of the incorporation of CeO_2 in the coatings during PEO, oxygen vacancies are created, which accounts for the increase in the PL intensity of $MgO/MgAl_2O_4/CeO_2$ coatings over pure $MgO/MgAl_2O_4$ coatings, as the PL originating from CeO_2 particles is barely noticeable.
- The content of CeO_2 particles in the aluminate electrolyte, i.e., the amount of CeO_2 particles incorporated within $MgO/MgAl_2O_4$ coatings, determines the PA of the $MgO/MgAl_2O_4/CeO_2$ coatings. The decrease in the photogenerated electron/hole recombination rate resulting from $MgO/MgAl_2O_4$ and CeO_2 coupling is linked to the increased PA of $MgO/MgAl_2O_4/CeO_2$. The $MgO/MgAl_2O_4/CeO_2$ coating formed in aluminate electrolyte with the addition of 2 g/L CeO_2 particles exhibits the highest PA.
- The PA, morphology, and composition of the formed photocatalysts did not alter after multiple PA cycles, indicating their chemical and physical stability, which is a crucial requirement for any potential applications.

Author Contributions: Conceptualization, S.S.; methodology, S.S. and N.R.; validation, S.S., investigation, S.S. and N.R.; writing—original draft preparation, S.S. and N.R.; writing—review and editing, S.S. All authors have read and agreed to the published version of the manuscript.

Funding: This research was funded by the Ministry of Education, Science, and Technological Development of the Republic of Serbia (grants 451-03-65/2024-03/200162 and 451-03-68/2023-14/200026) and by the European Union Horizon 2020 Research and Innovation program under the Marie Sklodowska-Curie grant agreement no. 823942 (FUNCOAT).

Data Availability Statement: The original contributions presented in the study are included in the article, further inquiries can be directed to the corresponding author.

Conflicts of Interest: The authors declare no conflicts of interest.

References

1. Kaseem, M.; Fatimah, S.; Nashrah, N.; Ko, Y.G. Recent progress in surface modification of metals coated by plasma electrolytic oxidation: Principle, structure, and performance. *Prog. Mater. Sci.* **2021**, *117*, 100735. [CrossRef]
2. Simchen, F.; Sieber, M.; Kopp, A.; Lampke, T. Introduction to plasma electrolytic oxidation—An overview of the process and applications. *Coatings* **2020**, *10*, 628. [CrossRef]
3. Tsai, D.-S.; Chou, C.-C. Review of the soft sparking issues in plasma electrolytic oxidation. *Metals* **2018**, *8*, 105. [CrossRef]
4. Sikdar, S.; Menezes, P.V.; Maccione, R.; Jacob, T.; Menezes, P.L. Plasma electrolytic oxidation (PEO) process—Processing, properties, and applications. *Nanomaterials* **2021**, *11*, 1375. [CrossRef]
5. Clyne, T.W.; Troughton, S.C. A review of recent work on discharge characteristics during plasma electrolytic oxidation of various metals. *Int. Mater. Rev.* **2019**, *64*, 127–162. [CrossRef]
6. Yang, Y.; Xiong, X.; Chen, J.; Peng, X.; Chen, D.; Pan, F. Research advances of magnesium and magnesium alloys worldwide in 2022. *J. Magnes. Alloys* **2023**, *11*, 2611–2654. [CrossRef]
7. Tan, J.; Ramakrishna, S. Applications of magnesium and its alloys: A review. *Appl. Sci.* **2021**, *11*, 6861. [CrossRef]
8. Esmaily, M.; Svensson, J.E.; Fajardo, S.; Birbilis, N.; Frankel, G.S.; Virtanen, S.; Arrabal, R.; Thomas, S.; Johansson, L.G. Fundamentals and advances in magnesium alloy corrosion. *Prog. Mater. Sci.* **2017**, *89*, 92–193. [CrossRef]
9. Gray, J.E.; Luan, B. Protective coatings on magnesium and its alloys—A critical review. *J. Alloys Compd.* **2002**, *336*, 88–113. [CrossRef]
10. Zhao, C.; Wang, X.; Yu, B.; Cai, M.; Yu, Q.; Zhou, F. Research progress on the wear and corrosion resistant plasma electrolytic oxidation composite coatings on magnesium and its alloys. *Coatings* **2023**, *13*, 1189. [CrossRef]
11. Darband, G.B.; Aliofkhazraei, M.; Hamghalam, P.; Valizade, N. Plasma electrolytic oxidation of magnesium and its alloys: Mechanism, properties and applications. *J. Magnes. Alloys* **2017**, *5*, 74–132. [CrossRef]
12. Whitea, L.; Koo, Y.; Neralla, S.; Sankar, J.; Yun, Y. Enhanced mechanical properties and increased corrosion resistance of a biodegradable magnesium alloy by plasma electrolytic oxidation (PEO). *Mater. Sci. Eng. B* **2016**, *208*, 39–46. [CrossRef]
13. Usmaniya, N.; Pillai, S.R.; Edalacheruvu, L.; Palanivel, M.; Chennampalli, P.; Vaithiyanathan, P.; Parfenov, E.; Lingamaneni, R.K.; Nagumothu, R. Effect of polycaprolactone coating on the corrosion and biological characteristics of plasma electrolytic oxidised ZM21 magnesium alloy. *Surf. Coat. Technol.* **2023**, *471*, 129915. [CrossRef]
14. Fattah-alhosseini, A.; Molaei, M.; Nouri, M.; Babaei, K. Antibacterial activity of bioceramic coatings on Mg and its alloys created by plasma electrolytic oxidation (PEO): A review. *J. Magnes. Alloys* **2022**, *10*, 81–96. [CrossRef]
15. Kumara, S.; Katyala, P.; Chaudhary, R.N.; Singh, V. Assessment of factors influencing bio-corrosion of magnesium-based alloy implants: A review. *Mater. Today Proc.* **2022**, *56*, 2680–2689. [CrossRef]
16. Kröger, N.; Kopp, A.; Staudt, M.; Rusu, M.; Schuh, A.; Liehn, E.A. Hemocompatibility of plasma electrolytic oxidation (PEO) coated Mg-RE and Mg-Zn-Ca alloys for vascular scaffold applications. *Mater. Sci. Eng. C* **2018**, *92*, 819–826. [CrossRef]
17. Husak, Y.; Olszaniecki, J.; Pykacz, J.; Ossowska, A.; Blacha-Grzechnik, A.; Waloszczyk, N.; Babilas, D.; Korniienko, V.; Varava, Y.; Diedkova, K.; et al. Influence of silver nanoparticles addition on antibacterial properties of PEO coatings formed on magnesium. *Appl. Surf. Sci.* **2024**, *654*, 159387. [CrossRef]
18. Patrascu, I.; Ducu, M.C.; Negrea, A.D.; Moga, S.G.; Plaiasu, A.G. Overview on plasma electrolytic oxidation of magnesium alloys for medical and engineering applications. *IOP Conf. Series Mater. Sci. Eng.* **2022**, *1251*, 012001. [CrossRef]
19. Tang, M.; Li, G.; Li, W.; Liu, H.; Zhu, L. Photocatalytic performance of magnesium alloy microarc oxides. *J. Alloys Compod* **2013**, *562*, 84–89. [CrossRef]
20. Li, W.; Tang, M.; Zhu, L.; Liu, H. Formation of microarc oxidation coatings on magnesium alloy with photocatalytic performance. *Appl. Surf. Sci.* **2012**, *258*, 10017–10021. [CrossRef]
21. Stojadinović, S.; Tadić, N.; Radić, N.; Grbić, B.; Vasilić, R. MgO/ZnO coatings formed on magnesium alloy AZ31 by plasma electrolytic oxidation: Structural, photoluminescence and photocatalytic investigation. *Surf. Coat. Technol.* **2017**, *310*, 98–105. [CrossRef]
22. Stojadinović, S.; Radić, N.; Vasilić, R. ZnO particles modified MgAl coatings with improved photocatalytic activity formed by plasma electrolytic oxidation of AZ31 magnesium alloy in aluminate electrolyte. *Catalysts* **2022**, *12*, 1503. [CrossRef]

23. Stojadinović, S.; Radić, N.; Vasilić, R. Photoluminescent and photocatalytic properties of Eu^{3+}-doped MgAl oxide coatings formed by plasma electrolytic oxidation of AZ31 magnesium alloy. *Coatings* **2022**, *12*, 1830. [CrossRef]
24. Supin, K.K.; Saji, A.; Chanda, A.; Vasundhara, M. Effects of calcinations temperatures on structural, optical and magnetic properties of MgO nanoflakes and its photocatalytic applications. *Opt. Mater.* **2022**, *132*, 112777.
25. Nitha, T.V.; Britto, S. $MgAl_2O_4$ nanospinel: Green synthesis, characterization and effective heterogeneous catalyst for the photocatalytic degradation of carbol fuchsin dye and synthesis of 2-aryl substituted benzoxazole derivatives. *Inorg. Chem. Commun.* **2024**, *159*, 111776. [CrossRef]
26. Kiran, N.; Baker, A.P.; Wang, G.-G. Synthesis and luminescence properties of MgO: Sm^{3+} phosphor for white light-emitting diodes. *J. Mol. Struct.* **2017**, *1129*, 211–215. [CrossRef]
27. Kumar, K.G.; Bhargav, P.B.; Aravinth, K.; Ahmed, N.N.; Balaji, C. Photoluminescence and electrochemical performance evaluation of Eu^{3+} doped $MgAl_2O_4$ phosphors for LED and energy storage applications. *Ceram. Int.* **2022**, *48*, 36038–36045. [CrossRef]
28. Mohedano, M.; Blawert, C.; Zheludkevich, M.L. Silicate-based plasma electrolytic oxidation (PEO) coatings with incorporated CeO2 particles on AM50 magnesium alloy. *Mater. Des.* **2015**, *86*, 735–744. [CrossRef]
29. Lim, T.S.; Ryu, H.S.; Hong, S.-H. Electrochemical corrosion properties of CeO_2-containing coatings on AZ31 magnesium alloys prepared by plasma electrolytic oxidation. *Corros. Sci.* **2012**, *62*, 104–111. [CrossRef]
30. Pan, J.; Wang, S.; Chen, A.; Chen, Y.; Wang, M.; Chen, Y. Visible-light-active mesoporous ceria (CeO_2) nanospheres for improved photocatalytic performance. *J. Alloys Compd.* **2022**, *898*, 162895. [CrossRef]
31. Kusmierek, E. A CeO2 semiconductor as a photocatalytic and photoelectrocatalytic material for the remediation of pollutants in industrial wastewater: A review. *Catalysts* **2020**, *10*, 1435. [CrossRef]
32. Pudukudy, M.; Jia, Q.; Yuan, J.; Megala, S.; Rajendran, R.; Shan, S. Influence of CeO_2 loading on the structural, textural, optical and photocatalytic properties of single-pot sol-gel derived ultrafine CeO_2/TiO_2 nanocomposites for the efficient degradation of tetracycline under visible light irradiation. *Mater. Sci. Semicond. Process.* **2020**, *108*, 104891. [CrossRef]
33. Habib, I.Y.; Burhan, J.; Jaladi, F.; Lim, C.M.; Usman, A.; Kumara, N.T.R.N.; Tsang, S.C.E.; Mahadi, A.H. Effect of Cr doping in CeO_2 nanostructures on photocatalysis and H_2O_2 assisted methylene blue dye degradation. *Catal. Today* **2021**, *375*, 506–513. [CrossRef]
34. Salimi, K. Self-assembled bio-inspired Au/CeO_2 nano-composites for visible white LED light irradiated photocatalysis. *Colloids Surf. A* **2020**, *559*, 124908. [CrossRef]
35. Wang, S.; Gao, H.; Li, J.; Wang, Y.; Chen, C.; Yu, X.; Tang, S.; Zhao, X.; Sun, G.; Li, D. Comparative study of the photoluminescence performance and photocatalytic activity of $CeO_2/MgAl_2O_4$ composite materials with an n-n heterojunction prepared by one-step synthesis and two-step synthesis methods. *J. Phys. Chem. Solids* **2021**, *150*, 109891. [CrossRef]
36. Matsukevich, I.; Kulinich, N.; Kulbitskaya, L.; Kuznetsova, T.; Popkov, V.; Chebanenko, M.; Moskovskikh, D.; Kuskov, K.; Romanovski, V. Mesoporous nanocomposites based on CeO_2 and MgO: Preparation, structure and photocatalytic activity. *J. Chem. Technol. Biotechnol.* **2023**, *98*, 2497–2505. [CrossRef]
37. Hoque, K.A.; Kumer, A.; Chakma, U.; Chowdhury, A.-N. Facile Synthesis of computationally designed $MgAl_2O_4/CeO_2/Cu_2O$ and $MgAl_2O_4/CeO_2/Ag_2O$ smart heterojunction photocatalysts for aqueous organic pollutants degradation. *ECS Trans.* **2022**, *107*, 13785–13796. [CrossRef]
38. Stojadinović, S.; Radić, N.; Perković, M. Highly efficient ZrO_2 photocatalysts in the presence of UV radiation synthesized in a very short time by plasma electrolytic oxidation of zirconium. *Opt. Mater.* **2023**, *146*, 114608. [CrossRef]
39. Rakoch, A.G.; Monakhova, E.P.; Khabibullina, Z.V.; Serdechnova, M.; Blawert, C.; Zheludkevich, M.L.; Gladkova, A.A. Plasma electrolytic oxidation of AZ31 and AZ91 magnesium alloys: Comparison of coatings formation mechanism. *J. Magnes. Alloys* **2020**, *8*, 587–600. [CrossRef]
40. Zimou, J.; Nouneh, K.; Hsissou, R.; El-Habib, A.; El Gana, L.; Talbi, A.; Beraich, M.; Lotfi, N.; Addou, M. Structural, morphological, optical, and electrochemical properties of Co-doped CeO_2 thin films, Mater. *Sci. Semicond. Process.* **2021**, *135*, 106049. [CrossRef]
41. Lua, X.; Mohedano, M.; Blawerta, C.; Matykina, E.; Arrabal, R.; Kainer, K.U.; Zheludkevich, M.L. Plasma electrolytic oxidation coatings with particle additions–A review. *Surf. Coat. Technol.* **2016**, *307*, 1165–1182. [CrossRef]
42. Orsetti, F.R.; Bukman, L.; Santos, J.S.; Nagay, B.E.; Rangel, E.C.; Cruz, N.C. Methylene blue and metformin photocatalytic activity of CeO_2-Nb_2O_5 coatings is dependent on the treatment time of plasma electrolytic oxidation on titanium. *Appl. Surf. Sci. Adv.* **2021**, *6*, 100143. [CrossRef]
43. Pathak, N.; Ghosh, P.S.; Gupta, S.K.; Mukherjee, S.; Kadam, R.M.; Arya, A. An insight into the various defects induced emission in $MgAl_2O_4$ and their tunability with phase behavior: Combined experimental and theoretical approach. *J. Phys. Chem. C* **2016**, *120*, 4016–4031. [CrossRef]
44. Choudhuryn, B.; Basyach, P.; Choudhury, A. Monitoring F, F^+, and F_2^{2+} related intense defect emissions from nanocrystalline MgO. *J. Lumin.* **2014**, *149*, 280–286. [CrossRef]
45. Pathak, N.; Ghosh, P.S.; Gupta, S.K.; Kadam, R.M.; Arya, A. Defects induced changes in the electronic structures of MgO and their correlation with the optical properties: A special case of electron–hole recombination from the conduction band. *RSC Adv.* **2016**, *6*, 96398. [CrossRef]
46. Zhang, J.; Zhang, L. Intensive green light emission from MgO nanobelts. *Chem. Phys. Lett.* **2002**, *363*, 293–297. [CrossRef]
47. Li, M.; Wang, X.; Li, H.; Di, H.; Wu, X.; Fang, C.; Yang, B. Preparation of photoluminescent single crystalline MgO nanobelts by DC arc plasma jet CVD. *Appl. Surf. Sci.* **2013**, *274*, 188–194. [CrossRef]

48. Uchino, T.; Okutsu, D.; Katayama, R.; Sawai, S. Mechanism of stimulated optical emission from MgO microcrystals with color centers. *Phys. Rev. B* **2009**, *79*, 165107. [CrossRef]
49. Lente, G. Facts and alternative facts in chemical kinetics: Remarks about the kinetic use of activities, termolecular processes, and linearization techniques, Curr. *Opin. Chem. Eng.* **2018**, *21*, 76–83. [CrossRef]
50. Fauzi, A.A.; Jalil, A.A.; Hassan, N.S.; Aziz, F.F.A.; Azami, M.S.; Hussain, I.; Saravanan, R.; Vo, D.-V.N. A critical review on relationship of CeO_2-based photocatalyst towards mechanistic degradation of organic pollutant. *Chemosphere* **2022**, *286*, 131651. [CrossRef] [PubMed]
51. Jing, L.; Qu, Y.; Wang, B.; Li, S.; Jiang, B.; Yang, L.; Fu, W.; Fu, H.; Sun, J. Review of photoluminescence performance of nano-sized semiconductor materials and its relationships with photocatalytic activity. *Sol. Energy Mater. Sol. Cells* **2006**, *90*, 1773–1787.